Journal of Building Engineering 114 (2025) 114303

Contents lists available at ScienceDirect

Journal of Building Engineering

journal homepage: www.elsevier.com/locate/jobe

The effect of seismic damage on the heating energy demand of buildings: A combined experimental study

D.A. Pohoryles, S. Kallioras, D.A. Bournas *

European Commission, Joint Research Centre (JRC), Ispra, Italy

ARTICLE INFO

Keywords:
Air infiltration
Blower-door test
Building energy consumption
Building energy modelling (BEM)
Seismic and energy assessment
Heating energy demand (HED)

ABSTRACT

This study addresses the yet underexplored impact of seismic damage on the energy efficiency of buildings, specifically focusing on air leakages and the resultant increases in heating energy demand. Recognising the combined need for seismic and energy retrofitting, it is important to better understand the effect of minor structural damage, such as earthquake-induced cracking, on the energy performance of existing buildings. This study presents for the first time a combined experimental study on these aspects of building performance. Novel findings from a series of consecutive earthquake and blower-door tests conducted on a full-scale, five-storey masonry-infilled reinforced concrete building are presented. Using a hybrid pseudo-dynamic testing approach that includes both physical and simulated components, the correlation between various extents of seismic damage and the corresponding air leakage rates is evaluated. Observations from earthquake tests are presented, and by means of blower door testing and thermal imaging, a connection between observed structural damage and air leakage metrics was confirmed. The experimental data was then used to conduct a detailed building energy modelling analysis, highlighting the broader implications of seismic damage on the heating energy demand of typical European mid-rise residential buildings. It was found that even low-level seismic damage can significantly affect a building's air tightness, leading to increased heating energy consumption. This research not only contributes to the understanding of seismic damage effects on the airtightness of building envelopes but also underscores the importance of integrated retrofitting strategies that consider both energy efficiency and seismic resilience to reduce environmental impact across the building life cycle.

1. Introduction

With the urgent need for renovating the existing building stock, the combination of seismic and energy retrofitting has been increasingly studied in recent years in order to tackle the issues of low energy efficiency and poor seismic performance of existing buildings with one intervention [1–4]. Recent earthquake events have shown that renovating buildings for energy efficiency alone can lead to additional unforeseen losses of the retrofitting investments if the seismic vulnerability of the building at hand is not also addressed [5]. Moreover, it has been recognised in the research community that seismic damage can lead to an increased environmental footprint due to greenhouse gas emissions and material waste associated with repair and demolition works [6–8]. A large area, including most of Southern and South-eastern, but also Central Europe, can be considered to have moderate to high seismic hazard,

* Corresponding author.
E-mail address: Dionysios.BOURNAS@ec.europa.eu (D.A. Bournas).

https://doi.org/10.1016/j.jobe.2025.114303
Received 8 March 2025; Received in revised form 2 September 2025; Accepted 5 October 2025
Available online 7 October 2025

with 30 % of European buildings located in areas where the peak ground acceleration (PGA) with a 10 % probability of exceedance in 50 years is at least 0.1g [9,10]. Renovating buildings with an integrated approach can hence achieve not only a reduction of the environmental footprint in the use phase of a building, i.e. due to reduced energy consumption, but also have a positive impact on the entire building life cycle due to the extension of its lifetime [11].

One issue that has, however, gained very little attention to date is the impact of low levels of damage caused by smaller earthquakes or ground settlements on the energy efficiency of existing buildings. Cracking of the building envelope, e.g. due to ageing and consequent material degradation, ground subsidence, and cumulative earthquake damage, can lead to increased air infiltration losses [12,13]. Typically, a distinction is made between diffuse air infiltration through small cracks in exterior walls or other envelope elements (making up around 18 %–50 % of air leakages), and concentrated infiltration, occurring at cracks around doors and windows (6 %–22 %) [14].

To date, only very limited research has been carried out to investigate the potential effect of earthquake damage on the air tightness of buildings. When a building sustains severe damage, e.g. on the scale where bricks in external walls are fractured, or external thermal insulation is detached, repair or reconstruction is needed. However, when only minor damage is observed (e.g. cracking to non-structural elements such as infill walls), often no repair works are carried out. In such cases, the presence of fine cracks may affect the future energy performance of the building due to air leakages. The effect on the air tightness of a building due to cracks in the envelope caused by earthquakes has however never been experimentally assessed at the building scale.

Research in this direction has mainly focussed on thick reinforced concrete (RC) walls of nuclear facilities, in which potential air leakages after earthquakes can have catastrophic outcomes [15,16]. More recently, two individual RC walls of different thicknesses have been tested under cyclic loading to increasing levels of damage to assess the effects of cracking on air tightness through the fan pressurisation method [17]. It was shown that the measured airflow coefficient would increase significantly with increased wall deformations and, hence, increased cracking. While this provides evidence for the need to further study the effect of seismic damage on air infiltration losses in buildings, these findings provide only localised information at the scale of an individual building element, but not at the building scale.

The air tightness of a building, measured by means of blower-door testing, can be directly correlated with its heating and cooling energy demand (HED and CED), as well as thermal comfort and moisture penetration [18]. Thermal losses through air infiltration are one of the highest contributors to heating and cooling energy consumption, next to the thermal transmission through external walls and roofs [19]. Depending on climatic conditions and building characteristics, losses through air infiltration can contribute around 20 % to the heating energy consumption of buildings [19]. These results have been corroborated by other studies, e.g. showing that overnormative air leakages result in about 20 % of overall energy use in buildings [20]. A study on the building stock in Amman showed that air infiltration can amount to 30 % of residential heating and cooling costs [18]. A correlation of energy performance and measured air-tightness was also obtained for buildings in China, where an increase of air changes per hour from 0.5 to 0.98 h^{-1} led to a 12.6 % increase in simulated HED [21]. Similarly, based on blower door test measurements in Spain, it was found that increased levels of air infiltration significantly impact the energy use of buildings, which, depending on local climatic conditions, can amount to nearly 25 % of the total HED [22]. Additionally, air infiltration can also be linked to increases in moisture penetration that can result in moisture accumulation problems in the building envelope due to localised moisture condensation [14].

Moreover, air infiltration through leaky building envelopes can be a source of penetration of outdoor PM2.5 particles e.g.: [23,24], as can meteorological factors and user behaviour (opening of windows) [25]. The risk of infiltration of outdoor PM2.5 particles through leaky envelopes is however depending on local outdoor air pollution, which depends heavily on the location of the building [26]. A review of 20 studies across different European, North American and Asian locations with different climatic conditions and outdoor pollutant levels [27] has shown that higher airtightness reduces infiltration of PM2.5 particles into dwellings in areas with high outdoor pollutant levels. The results were however inconclusive for locations with low pollution. Additionally, indoor air pollution is also highly dependent on multiple factors beyond airtightness, and may stem from indoor contaminants, e.g. from materials used in furnishings (such as Volatile Organic Compounds) or the type of paint applied on walls [28], but also occupant activities, such as cooking or smoking indoors [29,30]. Newer buildings may also face challenges related to indoor air quality due to pollutants of indoor origin, particularly when high levels of airtightness are not complemented by effective ventilation strategies or systems [31].

In this study, the effect of different levels of earthquake-induced damage on the air tightness of the building envelope is experimentally investigated on a full-scale structure. A full-scale five-storey masonry-infilled RC building was subjected to earthquake tests at the JRC's ELSA (European Laboratory for Structural Assessment) reaction wall facility using the pseudo-dynamic testing method with sub-structuring. In this hybrid testing approach, the bottom part of the structure (consisting of the first two storeys) was physically tested in the laboratory, while the three upper storeys were simulated numerically. A detailed discussion of the results from those tests is presented in Ref. [32].

This paper discusses the results from a series of blower-door tests (BDT) carried out at different damage levels of the building specimen. This combination of earthquake tests and air-infiltration tests on a full-scale building are the first of its kind in the academic literature. The damage sustained by the structure at each seismic intensity level is correlated with the air leakage measured during the BDT. The experimental results are then used to investigate the effect of seismic damage on the heating and cooling energy demand of a typical mid-rise RC building in the EU by means of building energy modelling (BEM).

2. Methodology

For the purpose of testing the effect of seismic damage to the building envelope on the energy efficiency of existing RC buildings with masonry infills, a series of full-scale experiments were carried out, consisting of hybrid earthquake and air infiltration tests. The

first were carried out using the pseudo-dynamic (PsD) testing method with sub-structuring, where part of the building (lower stories) was physically tested in the laboratory, and the rest (upper stories) was simulated numerically. Instead, the air tightness of the building envelope was measured through blower door tests (BDT) to identify potential air leakage through openings and cracks formed during the simulated earthquake sequence. Table 1 illustrates the order of the different tests performed on the building specimen. The table provides the input ground motion intensity—in terms of PGA for the earthquake tests. The building specimen, experimental setup, and testing protocol are described in the following sections.

Note that three cyclic quasi-static (pushover) tests were performed between the earthquake simulations to characterise the stiffness and hysteretic properties of the physical model. However, in each of these tests, the maximum inter-storey drift in the first storey remained below that of the preceding earthquake test. Therefore, the impact of the cyclic tests on cumulative damage (i.e., cracks on the building envelope) was considered minor. Nonetheless, it is reasonable to acknowledge that they may have contributed to slightly higher air infiltration in BDT2, BDT3, and BDT4.

2.1. Prototype building

The tests were carried out on a physical two-storey building portion shown in Fig. 1. It consists of two 4.0 m wide bays in the direction of testing (W-E) and one bay in the perpendicular direction (N-S). The first storey was fully infilled on all four sides with brick masonry walls, forming a closed room to carry out blower door tests. Note that the North side was infilled with double wythe masonry walls consisting of hollow 301 × 139 × 60 mm clay bricks (including a 130 mm wide gap), while the other three sides had a single wythe made from thicker 303 × 137 × 75 mm bricks. The North and South façades also included openings (Fig. 1C) for doors (0.90 m × 1.80 m) and windows (0.90 m × 1.20 m). The openings for doors in the first storey were sealed during the blower tests.

Material properties for the construction of the building prototype were obtained through tests on small-scale samples. Concrete of strength class C25/30 as per Eurocode 2 [33] was used for the RC frame, and an average compression strength of 38.3 MPa was obtained from compression tests on 12 standard 150-mm-size cubes. The steel rebars for reinforcement were of class B500C with a measured average yield strength of 530 MPa. For the masonry walls, the 60 mm and 75 mm thick hollow clay bricks had 49 % and 51 % void ratios and densities of 875 kg/m^3 and 855 kg/m^3, respectively. Their average compressive strengths in the direction parallel to the perforations were equal to 9.1 MPa and 8.2 MPa, respectively. The thermal resistance of the bricks was $R = 0.29$ m^{2}K/W for a unitary wall thickness of 80 mm, according to the technical sheets provided by the manufacturers.

Further details on the material strength testing, as well as the geometry and construction details of the building specimen, can be found in Ref. [32].

2.2. Hybrid earthquake testing

From a structural testing point of view, the building was subjected to hybrid earthquake testing (through the PsD testing method) [34,35]. Sub-structured pseudo-dynamic testing was carried out on a five-storey prototype structure consisting of a two-storey physical building (i.e., physical substructure), as shown in Fig. 1, while the upper three storeys were modelled numerically (i.e., numerical substructure). More information on the numerical sub-structuring and the seismic testing procedure is provided in a dedicated publication [32].

As shown in the test sequence in Table 1 and Fig. 2, a series of tests evaluating the structural performance and air tightness (blower door test) of the building was carried out. The six pseudo-dynamic tests simulated the effect of a ground motion from the 2016 Central Italy earthquake sequence. The selected accelerogram corresponds to the E-W component of the record at Castelluccio di Norcia station (IT-CLO-HGE), obtained from the engineering strong motion database (ESM) [36] and slightly modified in amplitude and frequency content to match the EC8 Type 1 spectrum for soil type B [37]. Spectral matching was necessary to ensure that the assessment was not tied to the specific site conditions, allowing for broader applicability of the results beyond a single recorded ground motion. More

Table 1
Summary of main earthquake simulations (EQ), cyclic pushover tests, and blower door tests (BDT).

Test type	Test name	PGA [g]
Air tightness	BDT 1	
Air tightness (sealed)	BDT 1*	
Pseudo-dynamic	EQ 1	0.10
Pseudo-dynamic	EQ 2	0.15
Cyclic quasi-static	PO 1	–
Air tightness	BDT 2	
Cyclic quasi-static	PO 2	–
Pseudo-dynamic	EQ 3	0.20
Pseudo-dynamic	EQ 4	0.20
Air tightness	BDT 3	
Pseudo-dynamic	EQ 5	0.25
Cyclic quasi-static	PO 3	–
Air tightness	BDT 4	
Pseudo-dynamic	EQ 6	0.30

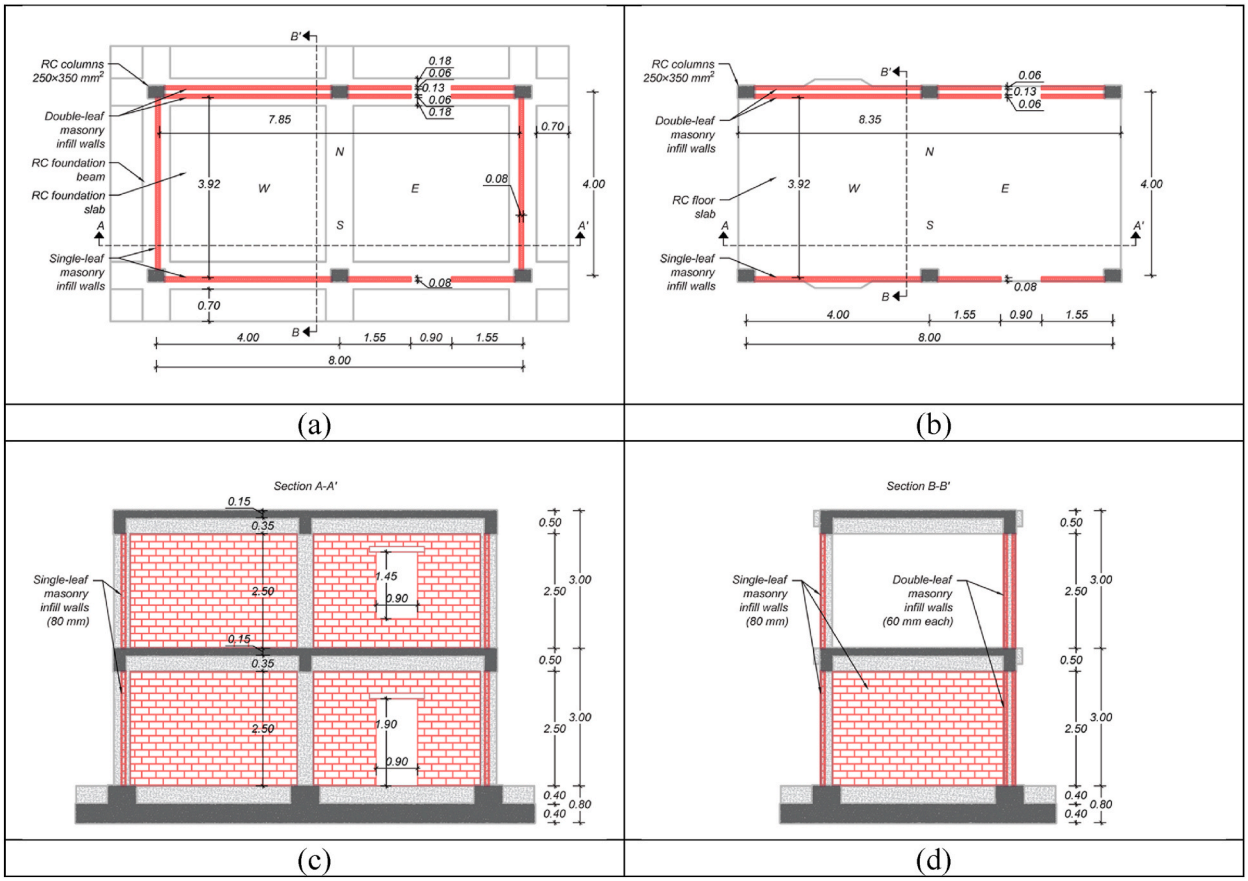

Fig. 1. Geometry of the test building: (a) ground-floor plan; (b) first-floor plan (c) elevation view in the longitudinal (i.e., X); building direction (d) elevation view in the transverse (i.e., Y); building direction. Units in m unless otherwise specified.

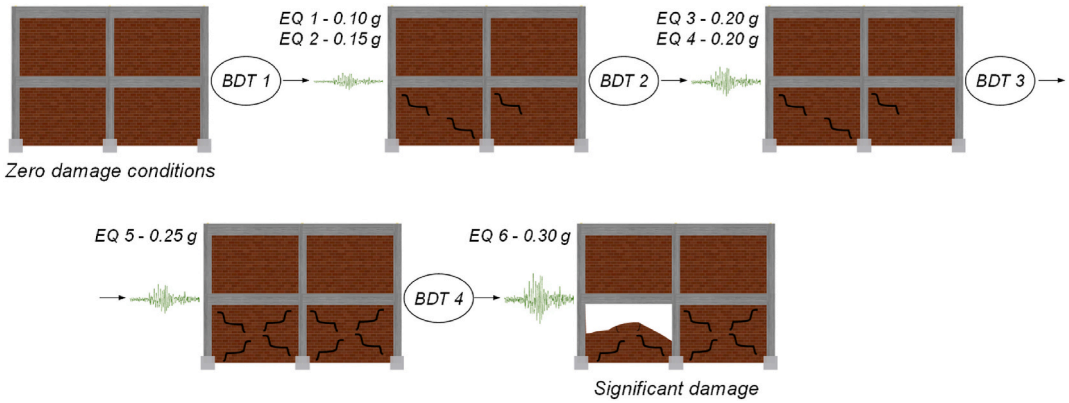

Fig. 2. Sequence of earthquake simulations and air tightness tests.

details on the ground motion can be found in the aforementioned [32]. The ground motion was then scaled to increasing intensity levels in terms of PGA, as shown in Table 1, ranging from 0.1 g to 0.3 g. Of interest to this study were the tests carried out up to a PGA of 0.25 g, for which blower door tests were also carried out to assess changes in air infiltration with increasing seismic damage.

2.3. Blower door testing

To measure the effect of seismic damage on the energy performance of the test building, as per Table 1, four blower door tests were

carried out. Specifically, one blower door test was performed before any earthquake test (at the undamaged state of the building), followed by three blower door tests, each carried out after subjecting the building to increasing levels of earthquake intensity, namely at PGAs of 0.15 g, 0.20 g, and 0.25 g. These tests measured the air tightness of a building at an applied pressure of 50 Pa and were performed according to ISO 9972: 2015 [38]. The pressure measurements of the blower door test equipment have a maximum measurement error of 3 %.

The equipment used for the test consists of one-way fans, a mounting frame, and relative sealings. The system was mechanically installed using adhesive tapes and without any perforation of the walls. Note that the blower door test was carried out exclusively at the first storey, with the pressure fan equipment installed on the door of the North façade (Fig. 3). The dimensions of the test structure relevant to the blower door measurements are listed in Table 2.

According to the to the ISO 9972:2015 protocol, readings of air flow are taken at least at five points of pressure for pressurisation and depressurisation. Here, the airflow rate through the fan and achieved building pressure are recorded at 10 pressure levels ranging from 10 to 55 Pa in increments of 5 Pa, as shown in Fig. 4 for BDT4. Based on these measurements, the leakage-pressure relationship of the test building (see Fig. 5) is established and used to derive the airflow at a differential pressure of 50 Pa (q_{50} in [m^3/h]).

After the initial blower door test (i.e., BDT1), air leakages in the first building storey were detected with a thermal infrared camera. To facilitate the detection of air infiltration, a temperature difference between the indoor (18.4 °C) and outdoor (16.4 °C) environments was established using a heating fan. Since the tests were conducted on a building specimen located inside the laboratory, the temperature difference was necessarily limited by the controlled indoor environment, preventing larger gradients typically achievable in outdoor field conditions. With the aim of accentuating and, therefore, facilitating the identification of any air infiltration, the blower door fan was activated to generate a pressure difference of 100 Pa between the internal and external environment. The surface temperatures were then measured with the infrared camera from outside the building, as shown in Fig. 6a. Under these conditions, it was possible to investigate sources of air leakage in the building envelope using thermal imaging (given the temperature difference between the heated inside air and the outside air temperature) and tracer smoke. Note that the latter has sensitivity limitations, especially in the case of small cracks and very airtight buildings.

The detection process identified leaks around the door (Fig. 6b) and at the anchorage system holes (Fig. 6c) at the foundation level. These openings were sealed to prevent unintended air losses unrelated to earthquake testing in subsequent experiments. In order to account for these losses in the undamaged building configuration, the blower door test was repeated after sealing the door and foundation holes to quantify air leakages from these sealed locations (test BDT1*). Instead, the pressure difference was brought to −50 and + 50 Pa, at which point airflow measurements were taken. For each subsequent blower door test, tracer smoke tests were conducted to identify new sources of air infiltration caused by increasing levels of seismic damage.

3. Experimental results

3.1. Damage observation and identification through thermal imaging

This section describes the observed damage on the external envelope of the test building, focusing only on the damage resulting from the pseudo-dynamic test directly preceding each blower door test. Table 3 provides the crack pattern observed on the masonry infills alongside the PGA intensity, first peak inter-storey drift ratio ($\delta_{1,max}$), and diagonal strain on the masonry infill walls ($\varepsilon_{d,max}$) caused by each PsD test. Note that only the damage in the first storey, i.e., where the blower door tests were carried out, is of relevance to the present study. In the earthquake tests relevant to the blower door tests, the test building was in damage conditions classified as DS1 and DS2, corresponding to no structural (or non-structural damage) and minor structural damage (or moderate non-structural damage), respectively, as defined in Kallioras et al. [32].

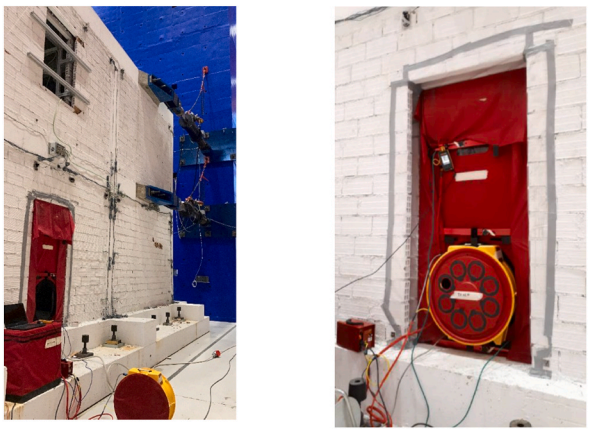

Fig. 3. Blower door test setup for airtightness tests on the full-scale building (a) overall view; (b) blower door fan.

Table 2
Relevant dimensions of the structure for the blower door testing.

Net volume	m^3	95.4
Enclosure height	m	3.3
Net floor area	m^2	30.7
Enclosure surface	m^2	138.3

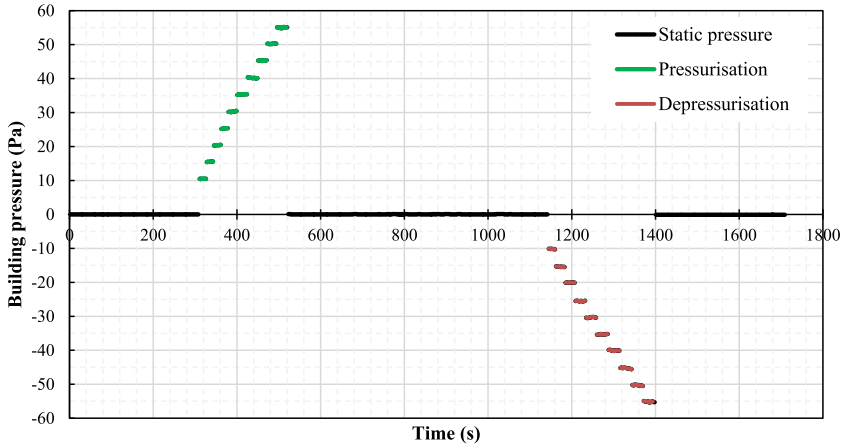

Fig. 4. Pressurisation and depressurisation protocol (representative example of BDT4).

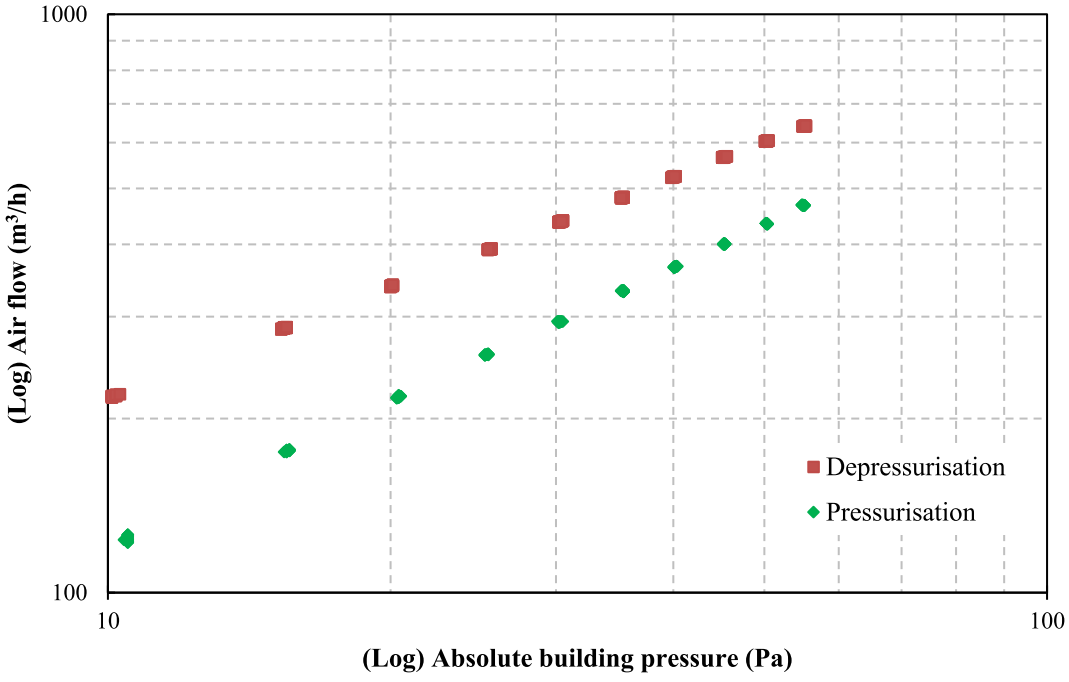

Fig. 5. Air leakage-pressure relationship of the test building (for BDT4) in log-scale.

The first BDT (BDT1) was carried out before subjecting the structure to earthquake testing, i.e., when the building had no damage. As shown in Fig. 6a, the only point of significant local air leakage was around the doors, which were consequently sealed. Through thermal imaging and the use of tracer smoke, it was further confirmed that no leakage through cracks occurred after the sealing of the door and the holes at the foundation level.

The first pseudo-dynamic tests preceding BDT2 were conducted at PGAs of 0.10 g and 0.15 g. In these tests, only slight to moderate non-structural damage was observed (classified as DS1), characterised by cracks along the interfaces between infills and the RC frame.

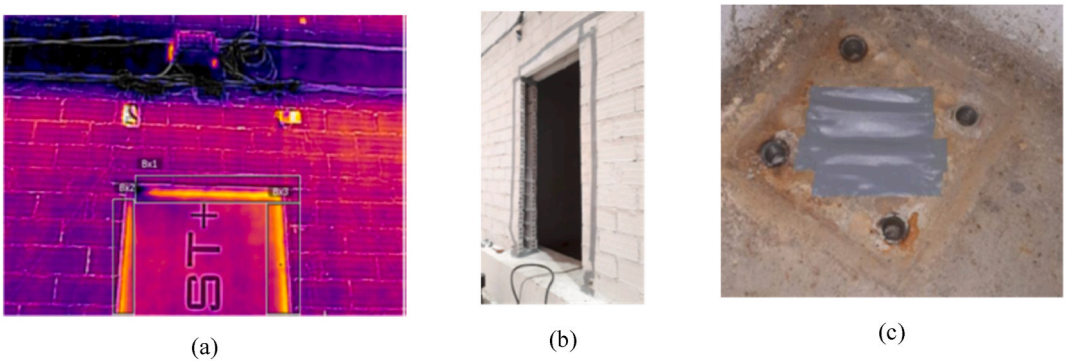

Fig. 6. (a) Air leakage and thermal bridge detection through thermal imaging; (b) sealing around the doors and (c) sealing at the foundation.

Table 3
Damage to the masonry infill walls observed at the end of the annotated PsD test (preceding the blower door tests BDT2, BDT3, and BDT4).

Seismic intensity	Inter-storey drift ratio	Diagonal strain on infill walls	Damage observation	
PGA [g]	$\delta_{1,max}$ [%]	$\varepsilon_{d,max}$ [%]	South façade	North façade
0.15	0.09	0.04	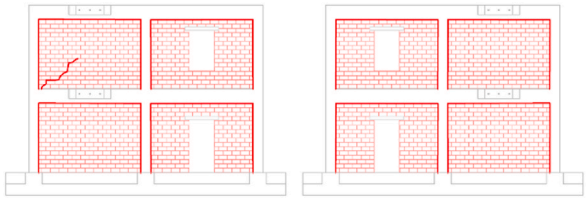	
0.20	0.23	0.12	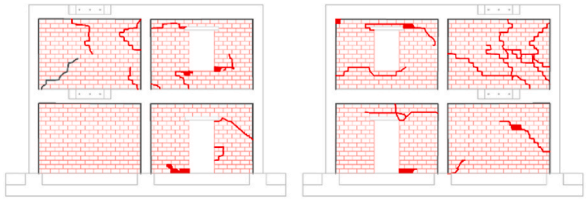	
0.25	0.39	0.21	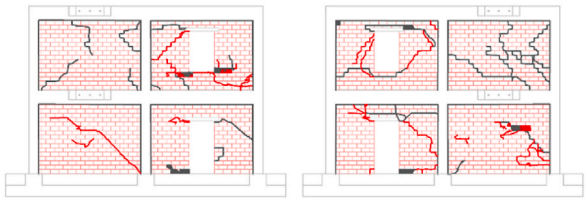	

The peak drift ratio ($\delta_{1,max}$) recorded at the first storey during the PGA = 0.15 g test was 0.089 %, and the maximum diagonal strain in the infills was 0.04 %. Through tracer smoke testing (Fig. 7a), the presence of cracks at the infill-frame interfaces of the transverse East and West infill walls was also confirmed. Thermal imaging highlighted additional small leakage areas on the surface of the infills, particularly at their corners, as shown in Fig. 7b.

The damage observed before BDT3, stemming from the PGA = 0.2 g tests, included larger infill-frame separation with increased crack widths at the corners highlighted by the tracer smoke tests and thermal imaging in Fig. 8. The increase in diagonal strain in the infill panels ($\varepsilon_{d,max}$ = 0.12 %) led to cracking due to tensile stresses at the centre and slight crushing due to compression at the corners of the infill panels, as visible in the thermal image in Fig. 8c. As shown in Fig. 8(e) and (f), cracking at the frame-infill interfaces was also observed at the East and West infill walls due to their out-of-plane response. This was also confirmed by the observation of escaping smoke in Fig. 8(a) and (b). Overall, the residual crack widths on the infills of the first storey did not exceed 2 mm, and the building would remain fully operational with possible minor repairs (DS2).

More significant leakage was detected after the PGA = 0.25 g earthquake simulation, i.e., preceding BDT4, as shown in Fig. 9. Severe leakage could be observed in the tracer smoke tests at the corners of the openings (Fig. 9a). Thermal imaging further revealed significant diagonal cracking on the infill between the RC column and the door (Fig. 9d), horizontal cracking along the infill-beam

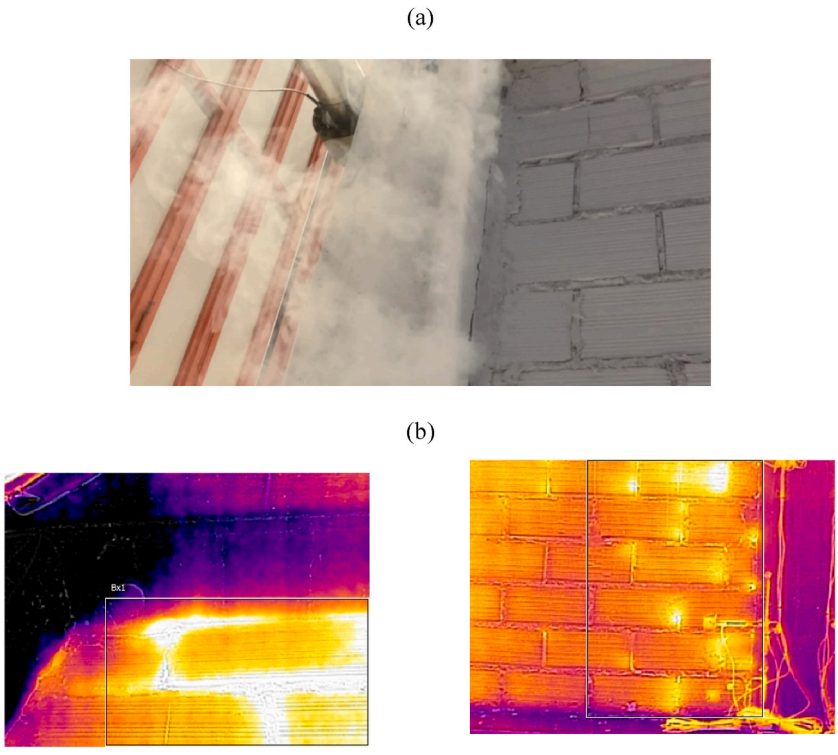

Fig. 7. Observed air leakage areas after BDT2: (a) air infiltration at the infill-frame interface visualised by tracer smoke, (b) crack detection at the infill corners through thermal imaging.

boundary (Fig. 9e), as well as damaged bricks in the fully infilled frame (without openings) (Fig. 9f). The peak diagonal strain recorded in the first storey infills reached 0.21 %, while the peak inter-storey drift was 0.39 %, both corresponding to a near doubling of the values recorded at the PGA = 0.2 g earthquake test.

Earthquake testing was continued up to a PGA of 0.3 g; however, at this point, the observed damage included significant spalling and crushing of bricks, with large holes in the masonry of the Southern infill walls. This level of damage would require extensive repair works in order to reuse the building, and is hence not relevant for the purpose of evaluating the effect of seismic damage on the energy consumption of the building. For a more detailed description of the structural damage assessment of the building, the reader is referred to Ref. [32].

3.2. Blower door test measurements and results

The results and testing conditions for the four air leakage tests are provided in Table 4. The table includes the intensity of the applied PSD test (in terms of PGA) preceding the blower door test, as well as the peak drift ratios at the first storey, $\delta_{1,max}$, attained during those tests. The table also provides the average internal and external temperature conditions during blower door testing. Additional quantities provided regard the airflow at a differential pressure of 50 Pa (q_{50} in [m^3/h]), the derived number of air changes per hour at a differential pressure of 50 Pa (n_{50}), i.e. the q_{50} value divided by the building volume (95.4 m^3), and the airflow rate through the building envelope at a differential pressure of 50 Pa ($q_{env,50}$ in [m^3/h/m^2]), i.e. the q_{50} value divided by the enclosure surface (138.3 m^2). The latter two quantities give an indication of the air tightness of the building, with a higher number of air changes corresponding to a leakier envelope [38]. An increased air permeability of the envelope in turn leads to a higher building energy consumption [39]. The maximum error of the obtained q_{50} values was ±4.2 %.

From all tests carried out, one can readily observe that an increase in seismic intensity and consequent structural damage leads to an increase in air leakage (Table 4). Specifically, air leakage, n_{50}, increased from 3.14 h^{-1} in the undamaged building to 5.47 h^{-1} after the PGA = 0.25 g earthquake test, corresponding to a 74 % increase in air change rate. Comparing the tests BDT1 and BDT1*, i.e., removing the effect of the air leakage around the door by fully sealing the gaps, an even clearer difference is noted, with the undamaged building having an n_{50} value of 1.81 h^{-1}. Looking at the measured airflow values, q_{50}, the leakages around the door accounted for 42.3 % of the overall leakages at undamaged building conditions. The difference between the n_{50} value at BDT4 and the estimated n_{50} for the undamaged building with the sealed door is 202 %.

As shown in Fig. 10, air leakages are well correlated with observed earthquake-induced damage to the building envelope, which in turn correlates well with higher recorded inter-storey drift ratios. This is because the air leakage during BDT originated mainly from cracks at the brick infill walls and infill-frame interfaces, as well as at the location of damaged infill bricks, as demonstrated by thermal

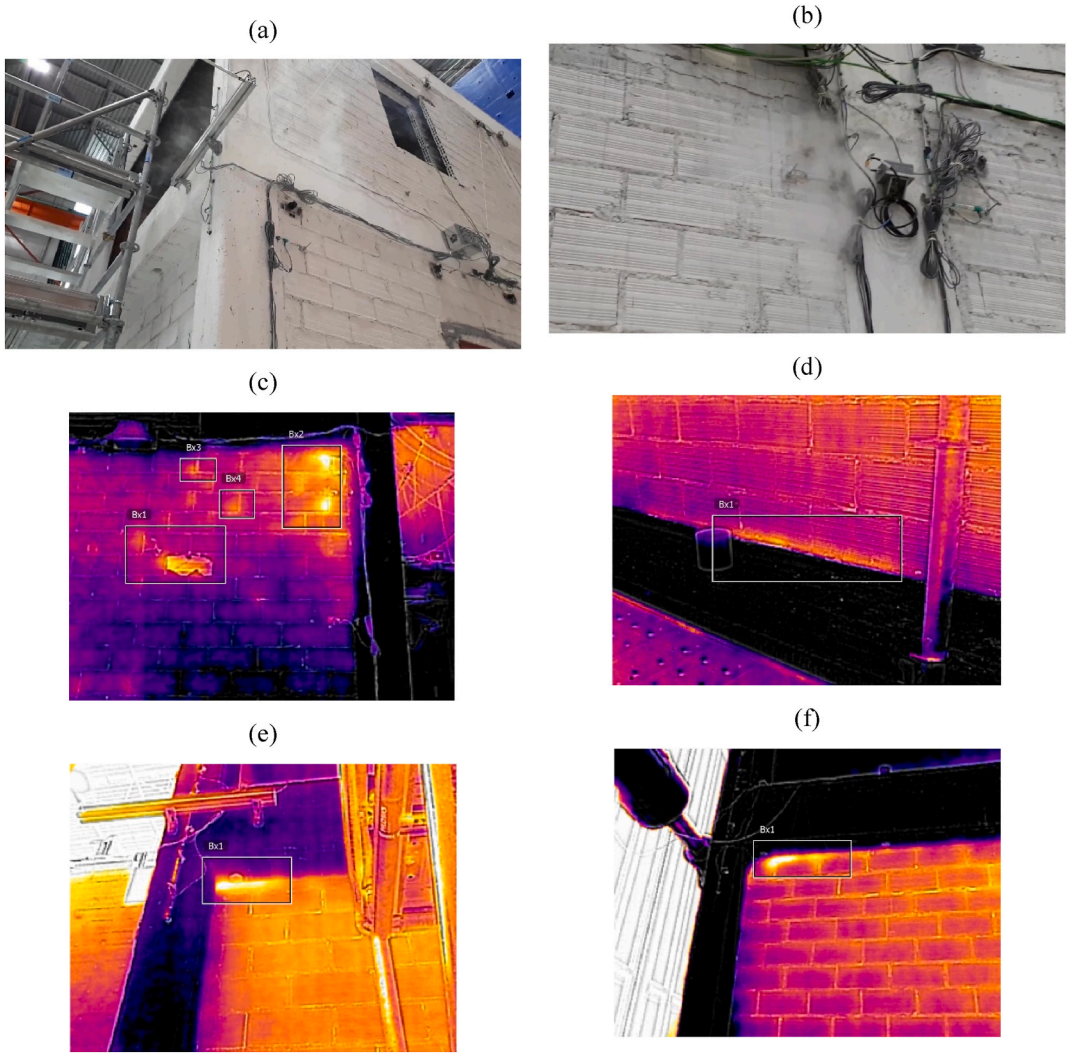

Fig. 8. Damage to the first storey masonry infills observed during BDT3, following the earthquake at PGA = 0.2 g: air infiltration at the infill-frame interface visualised by tracer smoke at the (a) exterior and (b) interior corner of the infill walls; (c)–(f) damage identification through thermal imaging: (c) crushing at the corners of the infills thermal imaging, (d) cracking along the base of the infill wall; (e)–(f) crack detection at the infill corners.

imaging.

According to the European standard EN 12831–1:2017 [40], the $q_{env,50}$ value can be used to differentiate between various airtightness levels/categories, where values below 2 $m^3/h/m^2$ correspond to high airtightness, and values between 3 and 6 $m^3/h/m^2$ to mid-level airtightness. As shown in Table 4, the original building, excluding infiltration losses around the door, would hence be categorised as a building with high airtightness, while for the final test, a mid-level category would be achieved.

In many EU countries, indicative limits for air infiltration for modern buildings are in place [39]. For instance, in Sweden, the airtightness of the building envelope in terms of $q_{env,50}$ for natural ventilation is limited to 2.4 $m^3/h/m^2$, while in Austria, an airtightness limit for natural ventilation in terms of n_{50} of 3.0 h^{-1} is prescribed. Therefore, before subjecting the test building to earthquake tests (in damage-free conditions), it was already around, or above, the limits of acceptable natural ventilation rates for many countries. As shown in Fig. 11, for most European countries where such limits exist, the n_{50} value obtained for the damaged building would be exceeded after the PGA = 0.2 g earthquake test (when n_{50} was 4.06).

4. Damage effect on heating energy demand

The effect of earthquake-induced damage on the airtightness of a building was clearly demonstrated by the blower door tests. This section quantifies how the reduction in airtightness resulting from seismic damage affects the HED of a case study multifamily building.

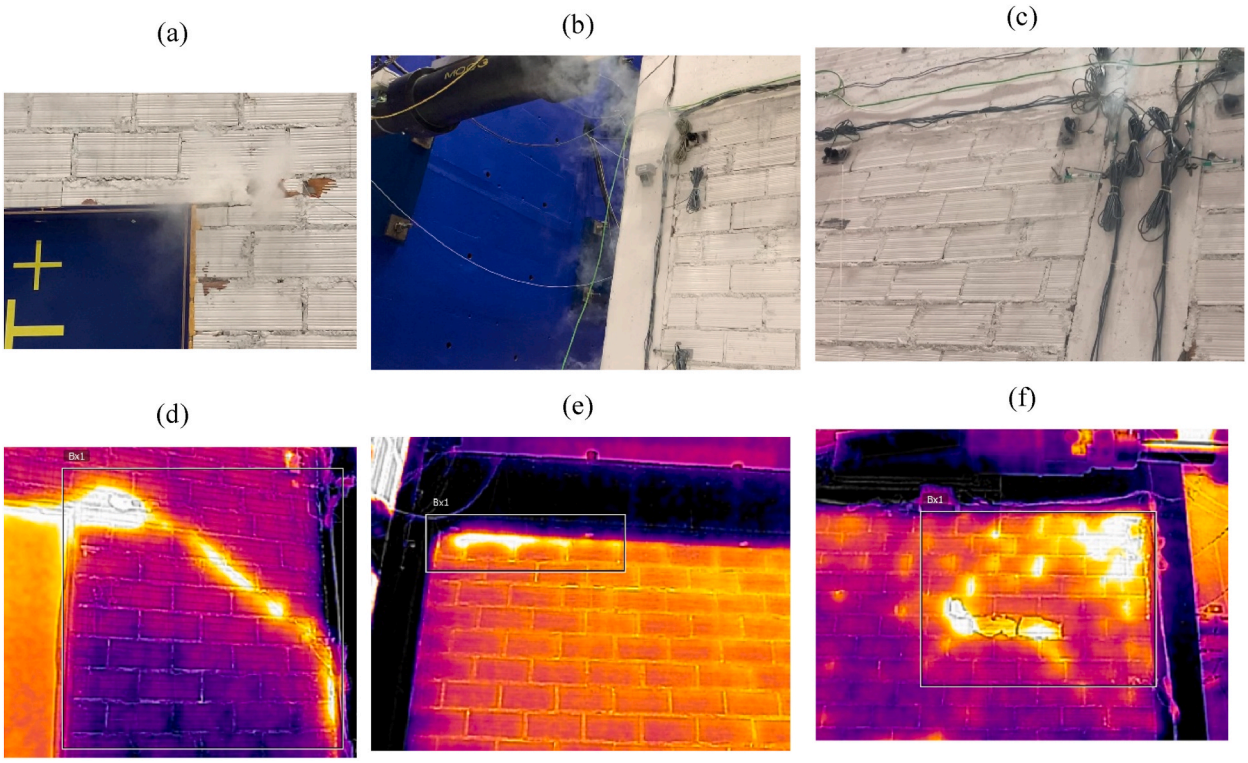

Fig. 9. Air leakage after the PGA = 0.25 g test: (a)+(d) through diagonal cracks in the infill wall; (b)+(e) through cracks at the beam-infill interface; (c)+(f) at the location of fractured bricks.

Table 4
Summary of measurements obtained from BDT (% error in parenthesis).

Test number	PGA	$\delta_{1,max}$	Indoor Temperature	Outdoor Temperature	q_{50}	n_{50}	$q_{env,50}$	Δq_{50}[b]
	[g]	[%]	[°C]	[°C]	[m^3/h]	[h^{-1}]	[$m^3/h/m^2$]	[%]
BDT 1	–	–	18.4	16.4	299.6	3.14	2.17	+73.2
BDT 1[a]	–	–	18.4	16.4	173.0	1.81	1.251	-
BDT 2	0.15	0.09	24.7	24.4	359.0	3.76	2.6	+107.4
BDT 3	0.20	0.23	25.5	25.4	387.3	4.06	2.8	+123.9
BDT 4	0.25	0.39	25.4	25.5	522.1	5.47	3.78	+201.7

[a] The door of the specimen was sealed for this test.
[b] Percentage difference for n_{50} and $q_{env,50}$ are equivalent, given that they are linearly derived from q_{50}.

4.1. *Building energy modelling assumptions*

The experimental results from the blower door tests are used as input for detailed BEM in EnergyPlus [42]. A mid-rise building was modelled at three different locations to account for varying climatic conditions and, accordingly, different Heating Degree Days (HDD), as shown in Table 5. The cities of Lisbon (Portugal), Perugia (Italy), and Sofia (Bulgaria) were selected to represent diverse climates: Lisbon corresponds to a mild Mediterranean climate with relatively low HDD, Perugia represents a temperate climate with moderate HDD, and Sofia reflects a continental climate with higher HDD, characterised by colder winters and greater heating demands.

HDD, calculated annually following the Eurostat methodology (Eq. (1) from Ref. [43]), accounts for different climatic conditions and, in particular, different ambient air temperatures, which is the primary factor influencing fluctuations in household energy use [44]. In symbols:

$$HDD = \sum_i \left(18^\circ C - T_m^i\right), \text{for } T_m^i \leq 15^\circ C \; HDD = 0, \text{for } T_m^i > 15^\circ C \tag{1}$$

where T_m^i is the mean air temperature of day *i*. In the detailed BEM, external climatic conditions are modelled using detailed *weather files* (typically 30-year climate records in format.*epw*) for the specific locations, as detailed in Table 5.

Another parameter influencing the overall thermal performance is the thermal transmittance—expressed in U-values in units W/

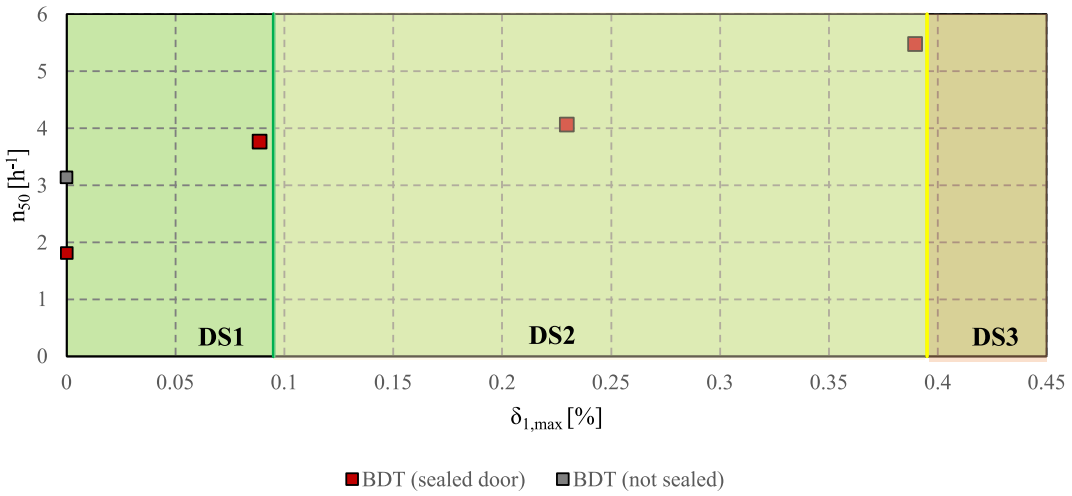

Fig. 10. Air leakage (n_{50}) against maximum inter-storey drift ratio at the first storey recorded at the prior earthquake tests with indication of the damage states (DS).

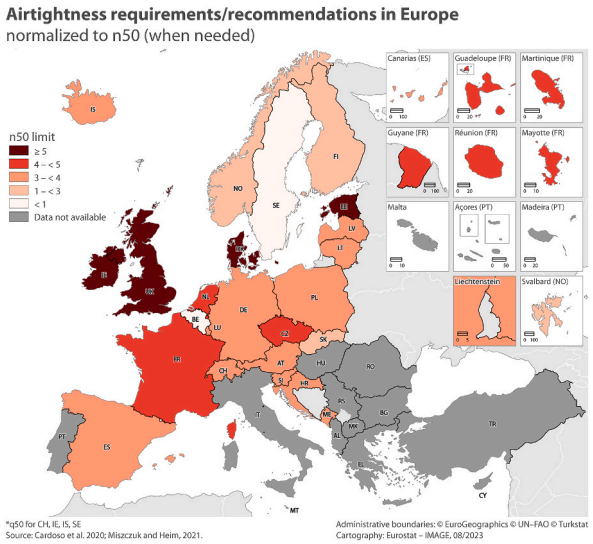

Fig. 11. Airtightness requirements/recommendations in Europe, in terms of n_{50} and $q_{env,50}$ (for CH, IE, IS and SE). Source [39,41].

Table 5
Heating degree days (HDD) and weather files in the selected case study European cities.

Location		Macro-climatic zone	HDD	Weather file ID	Source
Lisbon	Portugal	Mediterranean	900.8	PRT_Lisboa.085360_INETI	[45]
Perugia	Italy	Mediterranean	2129.5	ITA_Perugia.161810_IGDG	[46]
Sofia	Bulgaria	Continental	2976.1	BGR_Sofia.156140_IWEC	[47]

(m^2K)—of the various building elements, contributing significantly to heat transfer through the external walls and roof [48]. The selected features for evaluating their influence on the overall thermal performance of the building were the thermal transmittances (U-values in [$W/(m^2K)$]). The case study building was modelled with two different sets of U-values for walls and roof, reflecting cases of medium (U_{wall} = 1.33 W/m^2K, U_{roof} = 1.98 W/m^2K) and high (U_{wall} = 2.40 W/m^2K, U_{roof} = 2.11 W/m^2K) thermal transmittance. The associated U-values of windows and floors are shown in Table 6. These values were selected to represent average U-values implicitly including thermal bridges for buildings in EU countries with moderate-to-high seismic hazards, built between the 1960s and 1970s, usually without thermal insulation [49]. The full-scale building specimen discussed in these experiments represented this category of buildings.

Dynamic energy simulations were performed on the building model shown in Fig. 12 with ten time steps per hour, producing outputs for the annual space HED, normalised by the conditioned floor area (expressed as HED in units kWh/m^2/year). Based on previous work by some of the authors [3], the base area of the case study building was 8 × 18 m. Table 6 provides additional details, including storey height, roof type, and openings, as well as information on the glazing ratio and properties of windows, including their solar heat gain coefficient (SHGC)

Each floor of the building was modelled as a separate thermal zone, heated to a set point temperature of 20 °C (applied throughout the year). Ideal loads were assumed, neglecting the technical building system losses. As a result, the output energy demand can be considered to represent the useful energy demand. Internal heat gains from occupants, artificial lighting, electric equipment, and water heating were calculated using unit loads of 3.50 W/m^2, 8.00 W/m^2, 2.70 W/m^2 and 2.67 W/m^2, respectively, with hourly schedules adopted from Ref. [50]. More details on the geometry of the mid-rise case building, as well as energy modelling specifics such as schedules, material properties, and assumptions for internal heat gains, can be found in Refs. [3,50].

The building envelope composition that lead to the U-values for the walls and roof of the medium and high U-Value buildings are shown in Tables 7 and 8, respectively.

4.2. Heating energy demand calculations

The results from the BEM analyses are visualised in Fig. 13, showing changes in HED in kWh/m^2/year for the four experimentally determined levels of air infiltration (expressed in terms of air changes per hour, ACH). These results are provided for the two case study configurations—medium and high thermal transmittance, represented by the continuous and dashed lines, respectively—across three locations of different climatic conditions (in terms of HDD). Additionally, results are shown for the case of the initially undamaged building for which higher airtightness was achieved through sealing the door.

Table 9 summarises the results from the BEM analysis, showing the HED (kWh/m^2/y) for the two building configurations at three different sites, calculated for each experimentally measured ACH value. The table provides percentage differences in HED with respect to two airtightness levels of the undamaged building: with and without considering the effect of air leakages around the door and through the holes in the slab - reference experimental measurements from tests BDT1 and BDT1*, respectively. Given that the airtightness of a building reduces with age, the higher ACH value of BDT1 can be considered to more accurately represent an aged building.

The results listed in Table 9 indicate that the highest percentage increases in HED occur in Lisbon, particularly for buildings with lower thermal transmittance. This can be explained by the fact that the initial HED is lowest for these buildings (due to the very low HDD associated with the local climate conditions), and the increase in energy demand is predominantly driven by losses through air infiltration. For buildings of medium thermal transmittance, a 78 % increase (or 217 % compared to the sealed specimen) in energy consumption would be obtained for air infiltration associated with damage classified as DS2 (minor structural or moderate non-structural damage). However, at this damage level, repairs on the building envelope would likely be carried out. Still, even for lower damage levels such as DS1 (experimentally observed for a PGA = 0.2 g earthquake), air infiltration leads to a significant increase in HED: 30 % (or 132 % compared to the sealed building case). At this level of damage, repairs may not typically be performed in practice. For locations with higher HDD, i.e., Perugia (24 % or 103 %) and Sofia (23 % or 97 %), this percentage increase in HED is lower but remains substantial. Note that the analysis was also carried out for evaluating the CED for the medium U-value building for Lisbon and Sofia, however a maximum increase of 4.3 % (from 26.9 to 28.0 kWh/m^2/y) and 5.3 % (from 10.4 to 10.9 kWh/m^2/y), respectively, were obtained for the extreme values of ACH (1.81 and 5.47 h^{-1}). The impact of cracking on the CED was hence deemed not worthwhile for further investigation.

As expected, a building envelope with a higher U-value results in increased building energy consumption. The effect of losses due to air infiltration is however marginally less significant, despite the higher contribution of thermal transmission losses. Generally, it can be observed that for buildings with higher U-value, the relative impact of air infiltration on HED is reduced. The increase in HED due to

Table 6
Key parameters of building energy models.

Building properties	Thermal transmittance level	
	Medium	High
Base area [m^2]	8 x 18	
Total floor area [m^2]	576	
Number of storeys	4	
Storey height [m]	3	
Windows [m^2]	86.42	
External doors [m^2]	5.04	
Glazing [%]	15	
Roof type	Flat	
U_{wall} [W/m^{2}K]	1.33	2.40
U_{roof} [W/m^{2}K]	1.98	2.11
U_{floor} [W/m^{2}K]	1.4	2.5
U_{window} [W/m^{2}K]	3.5	5.5
SHGC	0.7	0.8

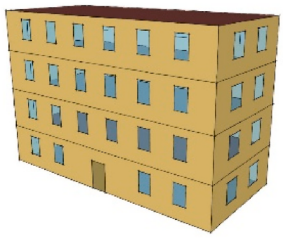

Fig. 12. Visualisation of building energy model.

Table 7
External wall material properties.

	Material	Thickness	Thermal conductivity	Density	Specific Heat	Thermal resistance	R-value[a]	U-Value
		t	λ	ρ	c	R_j	$R_{si}+\Sigma R_j+R_{se}$	1/R
		[m]	[W/mK]	[kg/m^3]	[J/kgK]	[m^{2}K/W]	[m^{2}K/W]	[W/m^{2}K]
Medium U-value	Wall plaster (mortar)	0.015	0.95	1700	840	0.0158	0.75	1.33
	Clay brick masonry	0.30	1.08	2150	870	0.2778		
	Stone wool board	0.01	0.036	60	840	0.2778		
	Wall plaster (mortar)	0.015	0.95	1700	840	0.0158		
High U-value	Wall plaster (mortar)	0.015	0.95	1700	840	0.0158	0.43	2.34
	Clay brick masonry	0.25	1.08	2150	870	0.2315		
	Wall plaster (mortar)	0.015	0.95	1700	840	0.0158		

[a] Note: The adopted method for estimating internal (R_{si}) and external (R_{se}) air surface resistances when calculating construction element U-values in EnergyPlus was DOE-2 and TARP, respectively [51].

Table 8
Roof material properties.

	Material	Thickness	Thermal conductivity	Density	Specific Heat	Thermal resistance	R-value[a]	U-Value
		t	λ	ρ	c	R_j	$R_{si}+\Sigma R_j+R_{se}$	1/R
		[m]	[W/mK]	[kg/m^3]	[J/kgK]	[m^{2}K/W]	[m^{2}K/W]	[W/m^{2}K]
Medium U-value	Heavyweight concrete	0.050	2.1	2240	900	0.0238	0.51	1.98
	Stone wool board	0.009	0.036	60	840	0.2528		
	RC slab	0.150	2.2	2500	840	0.0682		
	Ceiling plaster	0.020	0.96	1700	840	0.0208		
High U-value	Heavyweight concrete	0.050	2.1	2240	900	0.0238	0.48	2.11
	Stone wool board	0.008	0.036	60	840	0.2222		
	RC slab	0.150	2.2	2500	840	0.0682		
	Ceiling plaster	0.020	0.96	1700	840	0.0208		

[a] Note: The adopted method for estimating internal (R_{si}) and external (R_{se}) air surface resistances when calculating construction element U-values in EnergyPlus was DOE-2 and TARP, respectively [51].

air infiltration is less sensitive to the ACH for the higher U-value building envelopes compared to medium U-value envelopes. This difference is most accentuated when the air infiltration rate is lowest (ACH = 1.81), as the energy demand is predominantly driven by losses through thermal transmission.

5. Conclusions

This study assesses the impact of earthquake-induced damage on the energy performance of existing buildings. The focus is placed

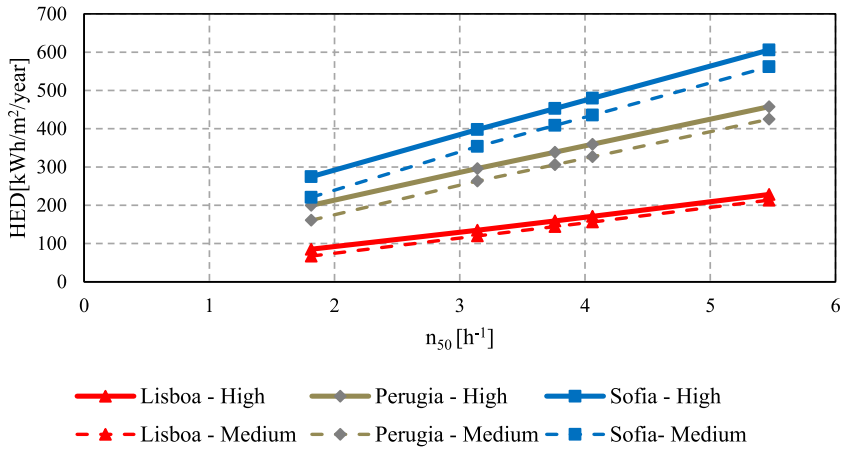

Fig. 13. Calculated heating energy demand (HED) for the medium and high thermal transmittance case study building with varying levels of air change rate (n_{50}).

Table 9
Calculated Heating Energy Demand (HED) for case study buildings with medium and high thermal transmittance (U-value) under varying air change rates.

City	ACH	Medium U-Value			High U-Value		
(HDD)	[h^{-1}]	HED [kWh/m^2/y]	vs. control[a]		HED [kWh/m^2/y]	vs. control[a]	
Lisbon (900.8)	1.81	67.24	−43.98 %	–	85.18	−36.76 %	–
	3.14	120.03	–	(78.50 %)	134.70	–	(58.13 %)
	3.76	144.32	20.24 %	(114.62 %)	159.09	18.11 %	(86.76 %)
	4.06	156.24	30.17 %	(132.35 %)	171.05	26.99 %	(100.80 %)
	5.47	213.39	77.78 %	(217.34 %)	228.22	69.43 %	(167.92 %)
Perugia (2129.5)	1.81	160.83	−38.91 %	–	199.80	−32.48 %	–
	3.14	263.26	–	(63.69 %)	295.90	–	(48.10 %)
	3.76	305.98	16.23 %	(90.25 %)	338.65	14.45 %	(69.49 %)
	4.06	326.74	24.11 %	(103.16 %)	359.42	21.47 %	(79.89 %)
	5.47	424.90	61.40 %	(164.20 %)	457.57	54.64 %	(129.01 %)
Sofia (2976.1)	1.81	220.78	−37.55 %	–	274.65	−30.93 %	–
	3.14	353.55	–	(60.14 %)	397.64	–	(44.78 %)
	3.76	408.71	15.60 %	(85.12 %)	452.76	13.86 %	(64.85 %)
	4.06	435.48	23.17 %	(97.25 %)	479.50	20.59 %	(74.59 %)
	5.47	561.77	58.89 %	(154.45 %)	605.68	52.32 %	(120.53 %)

[a] Comparison in parenthesis to BDT with a sealed door.

on typical European residential buildings made of masonry-infilled RC frames built between 1960 and 1970. Initially, the effect of seismic damage on the airtightness of a full-scale building envelope was assessed experimentally through a series of earthquake and airtightness tests. Subsequently, the study comprised building energy simulations to evaluate the relationship between various air tightness levels and heating energy consumption.

A series of earthquake tests of increasing intensity were performed on a full-scale building specimen using the pseudo-dynamic testing method. The tests brought the masonry infills of the test building to conditions of significant damage. The impact of earthquake-induced cracks and damage to the first-storey walls on the air infiltration was then assessed by means of blower-door tests. The latter were carried out for levels of damage that can be considered low to moderate, and were stopped once damage to the masonry infill walls was deemed irreparable (crushing and spalling of bricks).

As expected, increasing seismic intensity and the resulting cracking of the building envelope led to increased airflow and subsequent air leakage. Additionally, the observation of cracks in the infills through thermal imaging as well as through the creeping of tracer smoke through cracks proved very useful in determining the damage level after earthquake testing. Therefore, a potential application of the results presented here may also be the assessment of damage in masonry infills through non-destructive testing (NDT), e.g., by using a BDT to evaluate the degree of damage in a building after an earthquake. However, further experimental data collection and research are needed to develop such methodologies.

At a level of low to moderate seismic excitation (PGA = 0.15 g), when no significant damage to the structural or non-structural building elements (e.g., infill walls) was observed, a 20 % increase in air leakages (in terms of ACH) was recorded compared to the same building in undamaged conditions. This difference in ACH surged to 107 % compared to the undamaged building with a fully sealed door. After the earthquake test at PGA = 0.20 g, damage was still low, and would correspond to situations in which the building occupants may return to their homes without necessarily repairing them. The increase in ACH was slightly more significant (29 % and

124 % respectively). The building envelope would likely need reparation for more severe damage levels following an earthquake at PGA = 0.25 g, meaning that the obtained doubling in air infiltration would likely not be relevant.

Increases in air infiltration at different levels of non-structural damage measured through blower door tests were then correlated with potential increases in HED. Estimates of heating energy demand were obtained numerically by means of BEM at locations with different climatic conditions. Even for damage caused by a PGA = 0.15 g earthquake, increases in HED ranged between 65 % and 87 % for a building with high U-value (1.3 W/m^{2}K), and between 85 % and 115 % for a building with medium U-value (2.4 W/m^{2}K). This is a significant increase in energy demand for a level of damage that would likely not be repaired.

To mitigate energy losses in existing buildings exposed to low-to-moderate-intensity earthquakes, targeted interventions in the building stock are necessary. While building renovation should generally reduce air infiltration losses [52], it remains uncertain whether retrofitting can effectively prevent air infiltration caused by seismic damage. Retrofit techniques designed for the combined seismic and energy upgrading of buildings [53,54] should also be evaluated for their ability to maintain thermal performance over time by limiting air infiltration from repeated seismic events. Future studies on retrofitted structures should assess whether such techniques can provide a dual benefit, enhancing both seismic resilience and long-term energy efficiency.

CRediT authorship contribution statement

D.A. Pohoryles: Writing – original draft, Visualization, Validation, Software, Methodology, Investigation, Formal analysis, Data curation, Conceptualization. **S. Kallioras:** Writing – review & editing, Visualization, Validation, Project administration, Methodology, Investigation, Formal analysis, Data curation. **D.A. Bournas:** Writing – review & editing, Supervision, Resources, Project administration, Methodology, Investigation, Funding acquisition, Conceptualization.

Declaration of competing interest

The authors declare that they have no known competing financial interests or personal relationships that could have appeared to influence the work reported in this paper.

Acknowledgements

The experiment discussed in this paper was part of the research project '*iRESIST+ – Innovative seismic & energy retrofitting of the existing building stock*' sponsored by the European Commission's Joint Research Centre. The second and corresponding authors acknowledge funding from the European Union's Horizon 2020 research and innovation programme under the Marie Skłodowska-Curie grant agreement No 897822 — '*NOTICE-EUB - NOvel TImber CompositEs for Energy and seismic Upgrading of Buildings*'. The authors would like to thank M. Padovani and A. Caio for conducting out the blower door measurements. The contribution of the ELSA technical staff was critical to accomplishing the experimental activities and is also gratefully acknowledged.

Data availability

Data will be made available on request.

References

[1] G.M. Calvi, L. Sousa, C. Ruggeri, Energy efficiency and seismic resilience: a common approach, in: P. Gardoni, J.M. LaFave (Eds.), Multi-Hazard Approaches Civ. Infrastruct. Eng., Springer International Publishing, Cham, 2016, pp. 165–208, https://doi.org/10.1007/978-3-319-29713-2_9.
[2] D.A. Bournas, Concurrent seismic and energy retrofitting of RC and masonry building envelopes using inorganic textile-based composites combined with insulation materials: a new concept, Composites, Part B 148 (2018) 166–179, https://doi.org/10.1016/j.compositesb.2018.04.002.
[3] D.A. Pohoryles, C. Maduta, D.A. Bournas, L.A. Kouris, Energy performance of existing residential buildings in Europe: a novel approach combining energy with seismic retrofitting, Energy Build. 223 (2020) 110024, https://doi.org/10.1016/j.enbuild.2020.110024.
[4] D.A. Pohoryles, D.A. Bournas, F. Da Porto, A. Caprino, G. Santarsiero, T. Triantafillou, Integrated seismic and energy retrofitting of existing buildings: a state-of-the-art review, J. Build. Eng. 61 (2022) 105274, https://doi.org/10.1016/j.jobe.2022.105274.
[5] A. Belleri, A. Marini, Does seismic risk affect the environmental impact of existing buildings? Energy Build. 110 (2016) 149–158, https://doi.org/10.1016/j.enbuild.2015.10.048.
[6] G.A. Anwar, Y. Dong, Y. Li, Performance-based decision-making of buildings under seismic hazard considering long-term loss, sustainability, and resilience, Struct Infrastruct Eng 17 (2021) 454–470, https://doi.org/10.1080/15732479.2020.1845751.
[7] R.E. Gonzalez, M.T. Stephens, C. Toma, D. Dowdell, The estimated carbon cost of concrete building demolitions following the Canterbury earthquake sequence, Earthq. Spectra 38 (2022) 1615–1635.
[8] J. Xiao, Q. Deng, M. Hou, J. Shen, O. Gencel, Where are demolition wastes going: reflection and analysis of the February 6, 2023 earthquake disaster in Turkey, Low-Carbon Mater Green Constr 1 (2023) 17, https://doi.org/10.1007/s44242-023-00017-3.
[9] H. Crowley, V. Despotaki, D. Rodrigues, V. Silva, D. Toma-Danila, E. Riga, et al., Exposure model for European seismic risk assessment, Earthq. Spectra 36 (2020) 252–273, https://doi.org/10.1177/8755293020919429.
[10] K. Gkatzogias, H. Crowley, A. Veljkovic, D.A. Pohoryles, H. Norlén, G. Tsionis, et al., Prioritising EU Regions for Building Renovation: Seismic Risk, Energy Efficiency, Socioeconomic Vulnerability, Publications Office, 2022, https://doi.org/10.2760/263803. LU.
[11] L. Giresini, F. Stochino, M. Sassu, Economic vs environmental isocost and isoperformance curves for the seismic and energy improvement of buildings considering life cycle assessment, Eng. Struct. 233 (2021) 111923, https://doi.org/10.1016/j.engstruct.2021.111923.
[12] M.I. Montoya, E. Pastor, F.R. Carrié, G. Guyot, E. Planas, Air leakage in Catalan dwellings: developing an airtightness model and leakage airflow predictions, Build. Environ. 45 (2010) 1458–1469, https://doi.org/10.1016/j.buildenv.2009.12.009.
[13] M. Prignon, G. Van Moeseke, Factors influencing airtightness and airtightness predictive models: a literature review, Energy Build. 146 (2017) 87–97, https://doi.org/10.1016/j.enbuild.2017.04.062.

[14] C. Younes, C.A. Shdid, G. Bitsuamlak, Air infiltration through building envelopes: a review, J. Build. Phys. 35 (2012) 267–302, https://doi.org/10.1177/1744259111423085.
[15] S.P. Girrens, C.R. Farrar, Experimental Assessment of Air Permeability in a Concrete Shear Wall Subjected to Simulated Seismic Loading. United States, 1991.
[16] K. Okamoto, S. Hayakawa, R. Kamimura, Experimental study of air leakage from cracks in reinforced concrete walls, Nucl. Eng. Des. 156 (1995) 159–165, https://doi.org/10.1016/0029-5493(94)00941-Q.
[17] Y. Rokhyun, Y. Sanada, Y. Momoi, A study on airtight performance of cracked RC walls for building seismic performance evaluation, Proc 17th World Conf. Earthq. Eng. (2020) 11.
[18] K. Hassouneh, A. Alshboul, A. Al-Salaymeh, Influence of infiltration on the energy losses in residential buildings in Amman, Sustain. Cities Soc. 5 (2012) 2–7, https://doi.org/10.1016/j.scs.2012.09.004.
[19] F. Nemry, A. Uihlein, C.M. Colodel, B. Wittstock, A. Braune, C. Wetzel, et al., Environmental Improvement Potential of Residential Buildings IMPRO Building, Publications Office of the European Union, 2008.
[20] J. Šadauskienė, V. Paukštys, L. Šeduikytė, K. Banionis, Impact of air tightness on the evaluation of building energy performance in Lithuania, Energies 7 (2014) 4972–4987, https://doi.org/10.3390/en7084972.
[21] S. Chen, M.D. Levine, H. Li, P. Yowargana, L. Xie, Measured air tightness performance of residential buildings in North China and its influence on district space heating energy use, Energy Build. 51 (2012) 157–164, https://doi.org/10.1016/j.enbuild.2012.05.004.
[22] I. Poza-Casado, A. Meiss, M.Á. Padilla-Marcos, J. Feijó-Muñoz, Airtightness and energy impact of air infiltration in residential buildings in Spain, Int. J. Vent. 20 (2021) 258–264, https://doi.org/10.1080/14733315.2020.1777029.
[23] B. Stephens, J.A. Siegel, Penetration of ambient submicron particles into single-family residences and associations with building characteristics: particle penetration and building characteristics, Indoor Air 22 (2012) 501–513, https://doi.org/10.1111/j.1600-0668.2012.00779.x.
[24] N. Fu, M.K. Kim, L. Huang, J. Liu, B. Chen, S. Sharples, Experimental and numerical analysis of indoor air quality affected by outdoor air particulate levels (PM1.0, PM2.5 and PM10), room infiltration rate, and occupants' behaviour, Sci. Total Environ. 851 (2022) 158026, https://doi.org/10.1016/j.scitotenv.2022.158026.
[25] F. Zahed, A. Pardakhti, M.S. Motlagh, B. Mohammad Kari, A. Tavakoli, Infiltration of outdoor PM2.5 and influencing factors, Air Qual. Atmos. Health 15 (2022) 2215–2230, https://doi.org/10.1007/s11869-022-01246-4.
[26] E. Belias, D. Licina, Influence of outdoor air pollution on European residential ventilative cooling potential, Energy Build. 289 (2023) 113044, https://doi.org/10.1016/j.enbuild.2023.113044.
[27] L. Kempton, D. Daly, G. Kokogiannakis, M. Dewsbury, A rapid review of the impact of increasing airtightness on indoor air quality, J. Build. Eng. 57 (2022) 104798, https://doi.org/10.1016/j.jobe.2022.104798.
[28] E. Uhde, T. Salthammer, Impact of reaction products from building materials and furnishings on indoor air quality—A review of recent advances in indoor chemistry, Atmos. Environ. 41 (2007) 3111–3128, https://doi.org/10.1016/j.atmosenv.2006.05.082.
[29] R. Dales, L. Liu, A.J. Wheeler, N.L. Gilbert, Quality of indoor residential air and health, CMAJ Can Med Assoc J J Assoc Medicale Can 179 (2008) 147–152, https://doi.org/10.1503/cmaj.070359.
[30] J. Sundell, On the history of indoor air quality and health, Indoor Air 14 (Suppl 7) (2004) 51–58, https://doi.org/10.1111/j.1600-0668.2004.00273.x.
[31] J. Milner, I. Hamilton, C. Shrubsole, P. Das, Z. Chalabi, M. Davies, et al., What should the ventilation objectives be for retrofit energy efficiency interventions of dwellings? Build. Serv. Eng. Technol. 36 (2015) 221–229, https://doi.org/10.1177/0143624414566243.
[32] S. Kallioras, D.A. Pohoryles, D. Bournas, F.J. Molina, P. Pegon, Seismic performance of a full-scale five-story masonry-infilled RC building subjected to substructured pseudodynamic tests, Earthq. Eng. Struct. Dynam. 3940 (2023), https://doi.org/10.1002/eqe.3940.
[33] CEN. BS EN 1992-1-1:2004 Eurocode 2, Design of Concrete Structures, BSI, London, 2008. Part 1-1.
[34] G. Magonette, Development and application of large-scale continuous pseudo-dynamic testing techniques, Philos Trans R Soc Math Phys Eng Sci 359 (2001) 1771–1799, https://doi.org/10.1098/rsta.2001.0873.
[35] P. Pegon, J. Molina Ruiz Francisco, G. Magonette, Continuous pseudo-dynamic testing at ELSA. Hybrid Simul. Theory Implement. Appl., Taylor & Francis/Balkema, Leiden, The Netherlands, 2008, pp. 79–88.
[36] L. Luzi, G. Lanzano, C. Felicetta, M.C. D'Amico, E. Russo, S. Sgobba, et al., Engineering strong motion database (ESM), version 2.0, 2020. https://doi.org/10.13127/ESM.2.
[37] CEN. BS EN 1998-1:2004 Eurocode 8, Design of Structures for Earthquake Resistance - Part 1:General Rules, Seismic Actions and Rules for Buildings, BSI, London, 2004.
[38] ISO, ISO 9972:2015 Thermal Performance of Buildings. Determination of Air Permeability of Buildings. Fan Pressurization Method, CEN-CENELEC, Brussels, Belgium, 2015.
[39] A. Miszczuk, D. Heim, Parametric study of air infiltration in residential buildings—the effect of local conditions on energy demand, Energies 14 (2021) 127, https://doi.org/10.3390/en14010127.
[40] CEN. EN 12831-1:2017 Energy performance of buildings, Method for calculation of the design heat load. Space Heating Load, CEN-CENELEC, Brussels, Belgium, 2017. Module M3-3.
[41] V.E.M. Cardoso, P.F. Pereira, N.M.M. Ramos, R.M.S.F. Almeida, The impacts of air leakage paths and airtightness levels on air change rates, Buildings 10 (2020) 55, https://doi.org/10.3390/buildings10030055.
[42] U.S. Department of Energy, Energyplustm Version 9.5.0 Documentation Energyplus Essentials, U.S. Department of Energy, 2021.
[43] Eurostat, Energy Statistics - Cooling and Heating Degree Days (Nrg_Chdd). Ref. Metadata Euro SDMX Metadata Struct. ESMS, The Statistical Office of the European Union, Luxembourg, 2020.
[44] R.G. Quayle, H.F. Diaz, Heating degree day data applied to residential heating energy consumption, J. Appl. Meteorol. Climatol. 19 (1980) 241–246, https://doi.org/10.1175/1520-0450(1980)019<0241:HDDDAT>2.0.CO;2.
[45] INETI, Weather data by location, Reg - Eur WMO Reg 6 - Port Weather Data Download - Lisb 085360 INETI (2021). https://energyplus.net/weather-location/europe_wmo_region_6/PRT/PRT_Lisboa.085360_INETI.
[46] IGDG, Weather data by location, Reg - Eur WMO Reg 6 - Italy Weather Data Download - Perugia 161810 IGDG (2021). https://energyplus.net/weather-location/europe_wmo_region_6/ITA/ITA_Perugia.161810_IGDG.
[47] IWEC. Weather Data by Location, Reg - Eur WMO Reg 6 - Bulg Weather Data Download - Sofia 156140 IWEC (2021). https://energyplus.net/weather-location/europe_wmo_region_6/BGR/BGR_Sofia.156140_IWEC.
[48] Joint Research Centre, Institute for Prospective Technological Studies, F. Nemry, A. Uihlein, Environmental Improvement Potential of Residential Buildings: IMPRO Building, Office for Official Publications of the European Communities, Luxembourg, 2008.
[49] iNSPiRe, D2.1a - Survey on the Energy Needs and Architectural Features of the EU Building Stock, 2014.
[50] A. Veljkovic, D.A. Pohoryles, D.A. Bournas, Heating energy demand estimation of the EU building stock: combining building physics and artificial neural networks, Energy Build. 298 (2023) 113474, https://doi.org/10.1016/j.enbuild.2023.113474.
[51] U.S. Department of Energy, Energyplus Version 9.4.0 Documentation: Engineering Reference, U.S. Department of Energy, 2021.
[52] B. Milovanović, M. Bagarić, M. Gaši, M. Stepinac, Energy renovation of the multi-residential historic building after the Zagreb earthquake – case study, Case Stud. Therm. Eng. 38 (2022) 102300, https://doi.org/10.1016/j.csite.2022.102300.
[53] S. Kallioras, D. Bournas, L. Koutas, F.J. Molina, Integrated seismic and energy retrofitting of masonry-infilled RC buildings with textile-reinforced mortar and thermal insulation: full-scale tests on a five-story prototype, J. Build. Eng. (2024) 111006, https://doi.org/10.1016/j.jobe.2024.111006.
[54] S. Kallioras, D. Bournas, F. Smiroldo, I. Giongo, M. Piazza, F.J. Molina, Cross-laminated timber for seismic retrofitting of RC buildings: substructured pseudodynamic tests on a full-scale prototype, Earthq. Eng. Struct. Dynam. 4222 (2024), https://doi.org/10.1002/eqe.4222.